Anal. Chem. **2008,** *80,* 5293–5301

Articles

Energy Deposition during Molecular Depth Profiling Experiments with Cluster Ion Beams

Joseph Kozole,[†] Andreas Wucher,[‡] and Nicholas Winograd*[,†]

Department of Chemistry, Penn State University, 104 Chemistry Building, University Park, Pennsylvania 16802, and Department of Physics, University of Duisburg-Essen, Lotharstrasse 1, 47048 Duisburg, Germany

The role of the location of energy deposition during cluster ion bombardment on the quality of molecular depth profiling was examined by varying the incident angle geometry. Cholesterol films ~300 nm in thickness deposited onto silicon substrates were eroded using 40-keV C_{60}^+ at incident angles ranging from 5° to 73° with respect to the surface normal. The erosion process was evaluated by determining at each incident angle the total sputtering yield of cholesterol molecules, the damage cross section of the cholesterol molecules, the altered layer thickness within the solid, the sputter yield decay in the quasi-steady-state sputter regime, and the interface width between the cholesterol film and the silicon substrate. The results show that the total sputtering yield is largest relative to the product of the damage cross section and the altered layer thickness at 73° incidence, suggesting that the amount of chemical damage accumulated is least when glancing incident geometries are used. Moreover, the signal decay in the quasi-steady-state sputter regime is observed to be smallest at off-normal and glancing incident geometries. To elucidate the signal decay at near-normal incidence, an extension to an erosion model is introduced in which a fluence-dependent decay in sputter yield is incorporated for the quasi-steady-state regime. Last, interface width calculations indicate that at glancing incidence the damaged depth within the solid is smallest. Collectively, the measurements suggest that decreased chemical damage is not necessarily dependent upon an increased sputter yield or a decreased damage cross section but instead dependent upon depositing the incident energy nearer the solid surface resulting in a smaller altered layer thickness. Hence, glancing incident angles are best suited for maintaining chemical information during molecular depth profiling using 40-keV C_{60}^+.

The addition of cluster ion beam sources to traditional secondary ion mass spectrometry (SIMS) experiments has expanded the options for new applications. [1–5] One of the most important observations associated with these projectiles is that there is often very little chemical damage buildup during the interaction of the cluster with a molecular solid.[1–10] This effect is generally different from the behavior observed using atomic projectiles where damage buildup is usually quite severe, and the experiments must be carried out in either a low dose or very low kinetic energy (>200 eV) mode in order to retain the desired spectral information.[1–5,8,10,11] The high cleanup efficiency of cluster projectiles opens the possibility of molecular depth profiling through molecular solids, with many examples being reported in the past few years.[6–10,12–18] Buckminsterfullerene (C_{60}) has been shown to be particularly effective in this regard, although other cluster projectiles have also been shown to yield acceptable results.[12,14,16] If the cluster beam is focused to a submicrometer spot, it is feasible to create three-dimensional images of complex materials.[19,20] This application is particularly appealing to the biological imaging world, where the goal is to acquire three-

* To whom correspondence should be addressed. E-mail: nxw@psu.edu.
[†] Penn State University.
[‡] University of Duisburg-Essen.

(1) Appelhans, A. D.; Delmore, J. E. *Anal. Chem.* **1989**, *61*, 1087–1092.
(2) Gillen, G.; Simons, D. S.; Williams, P. *Anal. Chem.* **1990**, *62*, 2122–2130.
(3) Vickerman, J. C.; Briggs, D. *ToF-SIMS:Surface Analysis by Mass Spectrometry*; Surface Spectra: Manchester, 2001.
(4) Winograd, N. *Anal. Chem.* **2005**, *77*, 142A–149A
(5) Winograd, N.; Postawa, Z.; Cheng, J.; Szakal, C.; Kozole, J.; Garrison, B. J. *Appl. Surf. Sci.* **2006**, *252*, 6836–6843.
(6) Weibel, D. E.; Wong, S.; Lockyer, N.; Blenkinsopp, P.; Hill, R.; Vickerman, J. C. *Anal. Chem.* **2003**, *75*, 1754–1764.
(7) Wucher, A.; Sun, S.; Szakal, C.; Winograd, N. *Anal. Chem.* **2004**, *76*, 7234–7242.
(8) Sostarecz, A. G.; McQuaw, C. M.; Wucher, A.; Winograd, N. *Anal. Chem.* **2004**, *76*, 6651–6658.
(9) Mahoney, C.; Roberson, S.; Gillen, G. *Anal. Chem.* **2004**, *76*, 3199–3207.
(10) Wagner, M. S. *Anal. Chem.* **2005**, *77*, 911–922.
(11) Mine, N.; Douhard, B.; Brison, J.; Houssiau, L. *Rapid Commun. Mass Spectrom.* **2007**, *21*, 2680–2684.
(12) Touboul, D.; Kollmer, F.; Niehuis, E.; Brunelle, A.; Laprevote, O. *J. Am. Soc. Mass Spectrom.* **2005**, *16*, 1608–1618.
(13) Cheng, J.; Winograd, N. *Anal. Chem.* **2005**, *77*, 3651–3659.
(14) Cheng, J.; Wucher, A.; Winograd, N. *J. Phys. Chem. B* **2006**, *110*, 8329–8336.
(15) Fletcher, J.; Conlan, X. A.; Jones, E. A.; Biddulph, G. X.; Locklyer, N. P.; Vickerman, J. C. *Anal. Chem.* **2006**, *78*, 1827–1831.
(16) Jones, E. A.; Lockyer, N. P.; Vickerman, J. C. *Int. J. Mass Spectrom.* **2007**, *260*, 146–157.
(17) Shard, A. G.; Brewer, P. J.; Green, F. M.; Gilmore, I. S. *Surf. Interface Anal.* **2007**, *39*, 294–298.
(18) Shard, A. G.; Green, F. M.; Brewer, P. J.; Seah, M. P.; Gilmore, I. S. *J. Phys. Chem. B* **2008**, *112*, 2596–2605.
(19) Wucher, A.; Cheng, J.; Winograd, N. *Anal. Chem.* **2007**, *79*, 5529–5539.

10.1021/ac8002962 CCC: $40.75
Published on Web 06/13/2008

dimensional molecule-specific images of tissue or even single cells.

The physical phenomena that underlie molecular depth profiling experiments and the mathematical formulations necessary to characterize the parameters of the erosion process are only beginning to emerge. Recent molecular dynamics computer simulations suggest that, for C_{60}, energy deposition close to the sample surface yields the best possibility for molecular desorption.[21–27] To achieve this result, the models predict that glancing angles of incidence of the projectile will lead to the best outcome.[26,27] On the more phenomenological side, a semiquantitative erosion model has been developed that incorporates the total molecule sputtering yield, the damage cross section of the target molecule, and the altered layer thickness beneath the solid surface to describe the concentration of undamaged molecules as a function of the ion beam fluence.[14,18,28–30] This model suggests that the best molecular depth profiles are obtained when the total sputtering yield volume greatly exceeds the damaged volume per projectile impact, i.e., the product of the altered layer thickness with the damage cross section.[14,28] Since computer simulations in a companion study[27] predict that the altered layer thickness can be reduced at glancing angles of incidence without significant sacrifice of the total sputtering yield, both the calculation and the phenomenological model suggest that the angle of incidence of the projectile is an important parameter to consider.

Previous studies have utilized this erosion model to examine the influence of incident projectile kinetic energy and type on the quality of the molecular depth profile. For example, trehalose films dosed with small peptide molecules were eroded with Au^+, Au_2^+, and Au_3^+ clusters at 20 keV as well as with C_{60}^+ with kinetic energies ranging from 20 to 120 keV.[14,18,29,30] While each projectile except for Au^+ was shown to maintain a molecular ion signal during erosion, the C_{60}^+ projectile at 40 keV produced the cleanest depth profile.[14,30] This finding is consistent with a complementary study on water−ice overlayers, which shows that C_{60}^+ at large kinetic energies is the most appropriate ion beam parameter for molecular depth profiling.[24,31,32]

In this paper, the goal is to control the location of the energy deposition footprint during C_{60}^+ bombardment of a model organic thin film by varying the angle of incidence of the projectile from near-normal (5°) to glancing (73°). Using a ~300-nm cholesterol thin film as the model, we show that it is possible to extract the important parameters that describe the details of the depth profile itself and to see how these parameters depend upon the energy deposition process. For 40-keV C_{60}^+ bombardment, we find that the most glancing angles yield the largest sputtering yield volume relative to the damage volume and, hence, exhibit the highest cleanup efficiency.

The highest quality depth profiles are characterized by a steady-state molecular ion signal during the time when the molecular thin film is eroded by the ion beam. In most instances, however, a slight decrease of the signal is noted within this regime, yielding what might better be referred to as a "quasi steady state". Here, we also show that the nature of this quasi-steady-state region is highly dependent upon the angle of incidence of the primary ion beam. To elucidate the signal decay, an extension to the erosion model is introduced in which a fluence-dependent decay in sputter yield is incorporated. These corrections are ultimately shown to influence estimations of the maximum depth resolution achievable with the C_{60}^+ probe, a critical parameter in defining future applications of this approach.

EXPERIMENTAL SECTION

Sample analysis was performed using a TOF-SIMS instrument (BioToF, Kore Technology Ltd.) described previously.[33] A C_{60}^+ ion beam system (IOG-40, Ionoptika Ltd.) is operated at a 40-keV extraction voltage and is mounted onto the instrument at a 40° angle with respect to sample normal.[6,15,34] A 40-keV C_{60}^+ ion beam system is chosen since the parameters have been identified to be well-suited for molecular depth profiling.[14,30] Under typical operating conditions, the beam current is 200 pA and the beam size is 5 μm. The C_{60}^+ incident angle is varied between analyses using a customized sample mount, which can be used to adjust the target tilt in reference to the ion beam. Although this procedure prevents comparison of ion yields at different angles since the angle between the surface normal and the ion optical axis of the mass spectrometer also changes, ion yields acquired during a depth profile are comparable since the angle is kept constant during the data acquisition. Using the customized mount, the C_{60}^+ incident angle can be varied from 5° to 73°.

Cholesterol films were prepared on silicon substrates by physical vapor deposition (PVD) as described previously.[35] Cholesterol is chosen since the molecule is commonly used as a target in SIMS studies of biological samples.[12,16,36,37] The PVD process is initiated by heating a reservoir containing ~500 mg of cholesterol powder (Aldrich Chemical Co.) to ~200 °C. Subsequent to heating, cholesterol gas sublimes from the reservoir, passes through a defusing grid, and deposits onto a cryogenically cooled silicon substrate (Ted Pella Inc.). The films are characterized before and after analysis using atomic force microscopy (AFM, Nanopics 2100, TLA Tencor, Inc.).

An AFM image of a cholesterol film eroded using 40-keV C_{60}^+ at an incident angle of 40° is illustrated in Figure 1. The AFM measurement indicates a 4.7-nm root-mean-square film roughness over an area of 20 μm × 20 μm and a 277-nm film thickness. Similar values are observed at the other angles of incidence. Although,

(20) Fletcher, J. S.; Lockyer, N. P.; Vaidyanathan, S.; Vickerman, J. C. *Anal. Chem.* **2007**, *79*, 2199–2206.
(21) Postawa, Z.; Czerwinski, B.; Szewczyk, M.; Smiley, E. J.; Winograd, N.; Garrison, B. J. *J. Phys. Chem. B* **2004**, *108*, 7831–7838.
(22) Postawa, Z.; Czerwinski, B.; Winograd, N.; Garrison, B. J. *J. Phys. Chem. B* **2005**, *109*, 11973–11979.
(23) Russo, M. F., Jr.; Garrison, B. J. *Anal. Chem.* **2006**, *78*, 7206–7210.
(24) Russo, M. F.; Szakal, C.; Kozole, J.; Winograd, N.; Garrison, B. J. *Anal. Chem.* **2007**, *79*, 4493–4498.
(25) Smiley, E. J.; Wojciechowski, I. A.; Postawa, Z.; Winograd, N.; Garrison, B. J. *Appl. Surf. Sci.* **2006**, *252*, 6436–6439.
(26) Ryan, K. E.; Smiley, E. J.; Garrison, B. J., *Appl. Surf. Sci.* In press.
(27) Ryan, K. E.; Garrison, B. J. *Anal. Chem.* Submitted.
(28) Cheng, J.; Winograd, N. *Appl. Surf. Sci.* **2006**, *252*, 6498–6501.
(29) Wucher, A.; Cheng, J.; Winograd, N. *Appl. Surf. Sci.* In press.
(30) Wucher, A.; Cheng, J.; Winograd, N. *Anal. Chem.* To be submitted.
(31) Szakal, C.; Kozole, J.; Russo, M.F., Jr.; Garrison, B. J.; Winograd, N. *Phys. Rev. Lett.* **2006**, *96*, 216104−1216104−4.
(32) Szakal, C.; Kozole, J.; Winograd, N. *Appl. Surf. Sci.* **2006**, *252*, 6526–6528.
(33) Braun, R. M.; Blenkinsopp, P.; Mullock, S. J.; Corlett, C.; Willey, K. F.; Vickerman, J. C.; Winograd, N. *Rapid Commun. Mass Spectrom.* **1998**, *12*, 1246.
(34) Wong, S. C.; Hill, R.; Blenkinsopp, P.; Lockyer, N. P.; Weibel, D. E.; Vickerman, J. C. *Appl. Surf. Sci.* **2003**, *203*, 219–222.
(35) Willingham, D.; Kucher, A.; Winograd, N. *Appl. Surf. Sci.* In press.
(36) Sjovall, P.; Lausmaa, J.; Johansson, B. *Anal. Chem.* **2004**, *76*, 4271–78.
(37) Ostrowski, S. G.; Kurczy, M. E.; Roddy, T. P.; Winograd, N.; Ewing, A. G. *Anal. Chem.* **2007**, *79*, 3554–60.

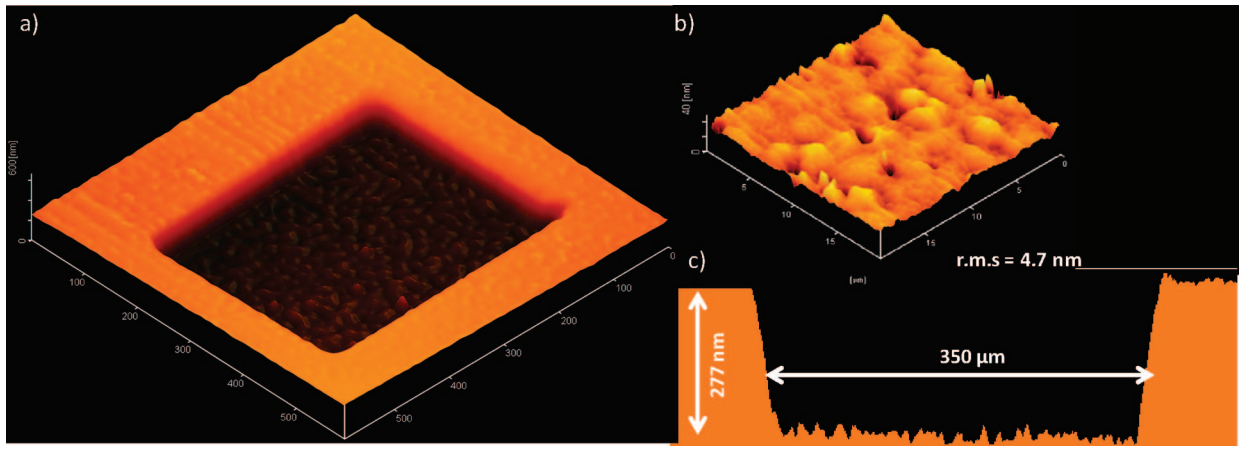

Figure 1. AFM images of a cholesterol film bombarded using 40-keV C_{60}^+ at 40° incidence. The AFM image in (a) is a three-dimensional representation of the bombarded region of the film taken from a 600 μm × 600 μm field. The AFM image in (b) is a three-dimensional representation of the unbombarded region of the film taken from a 20 μm × 20 μm field. The image measures the film to have a 4.7-nm rms roughness. The AFM image in (c) is a line scan taken across the bombarded region of the film. The image measures the film to have a 277-nm thickness.

the reason for the film roughness is currently unknown, a possible explanation involves film crystallization during deposition. Regardless of the reason, the film roughness measurement is highly reproducible day-to-day. The AFM measurement can also be used to determine the incident angle geometry of the bombardment. The ratio of the dimensions of the sputtered field is proportional to the incident angle geometry according to a cos θ relationship. Overall, the repeatability of the cholesterol films makes the sample a suitable platform for the routine comparison between molecular depth profiles acquired under varying conditions.

Molecular depth profile experiments were performed by alternating between erosion cycles and SIMS acquisition cycles as described earlier.[38] Briefly, erosion cycles involved rastering the C_{60}^+ ion beam across the sample in direct current (dc) mode. The sputter time (~2−3 s) and sputter field (~350 μm × 350 μm) were chosen to deliver ~1×10^{13} C_{60}^+ ions/cm^2 per erosion cycle. SIMS acquisition cycles involved rastering the C_{60}^+ ion beam in pulsed mode (~70-ns pulses, 3-kHz repetition rate) across the sample. The total ion fluence accumulated during an acquisition cycle was ~10^{11} cm^{-2} and could therefore safely be neglected even after taking hundreds of data points in a depth profile. To eliminate crater edge effects, the analysis field (~75 μm × 75 μm) was chosen to be smaller than the eroded field. Positive SIMS spectra were recorded in single ion counting mode and summed over 2×10^5 ion pulses. The depth profiles were characterized by plotting ion intensities from sequential spectra as a function of C_{60}^+ fluence. The plots are used to calculate a number of depth profile parameters, including the total sputtering yield, the damaged cross section of the molecule, the altered layer thickness, the sputter yield decay in the quasi-steady-state regime, and the interface width. Details for the calculations are provided in the discussion.

RESULTS AND DISCUSSION

The objective of this research is to control the location of the energy deposition footprint by varying the incident angle of the C_{60}^+ projectile and to determine the role of the location of the energy deposition upon the quality of the resulting molecular depth profile. Incident angles between 5° and 73° were chosen to illustrate the contrasting configurations of near-normal, off-normal, and glancing incident angle geometries. The results of the depth profiles are shown in Figure 2. The depth profiles are plots of cholesterol quasi-molecular ion (m/z = 369, $[M-H_2O]^+$) and silicon ion (m/z = 28, Si^+) intensities as a function of C_{60}^+ fluence. In general, the response of the cholesterol molecule signal has a similar trend for all incident geometries. Specifically, the trend is characterized by three separate regions: an initial loss of signal, an intermediate quasi steady state, and a complete disappearance of signal at the film/substrate interface. We did not observe an initial increase of the molecular ion signal as found during depth profiling of trehalose films.[13] This increase, presumably due to fluctuation of the ionization probability during formation of the altered layer, may be absent for the cholesterol films investigated here.

The extent of molecule response in each region, however, varies according to incident geometry. Most notably, the magnitude of the signal loss through the initial region and into the intermediate quasi-steady-state region decreases as the incident angle increases. The amount of chemical damage is smallest when the signal in the quasi-steady-state region is closest to the zero fluence value.[1,10,14,30,38] From this perspective, glancing incident angles, such as 73°, appear to be most effective for molecular depth profiling. To validate this observation and to understand the ion/solid interactions leading to this phenomenon, the degree of chemical damage in each experiment is evaluated using erosion dynamics.

Erosion dynamics have been discussed in detail previously.[14,18,28,30] Briefly, the model describes the concentration c_s of undamaged molecules within an altered layer of thickness d beneath the surface as a function of ion fluence f using the relationship

$$\frac{dc_s}{df} = \frac{Y^{tot}}{nd}(c_b - c_s) - \sigma_D c_s \quad (1)$$

where c_b is the bulk concentration of intact molecules, Y^{tot} is the total sputtering yield (in molecule equivalents removed per projectile impact), and n is the molecular density of the film. For

(38) Kozole, J.; Willingham, D.; Winograd, N. *Appl. Surf. Sci.* In press.

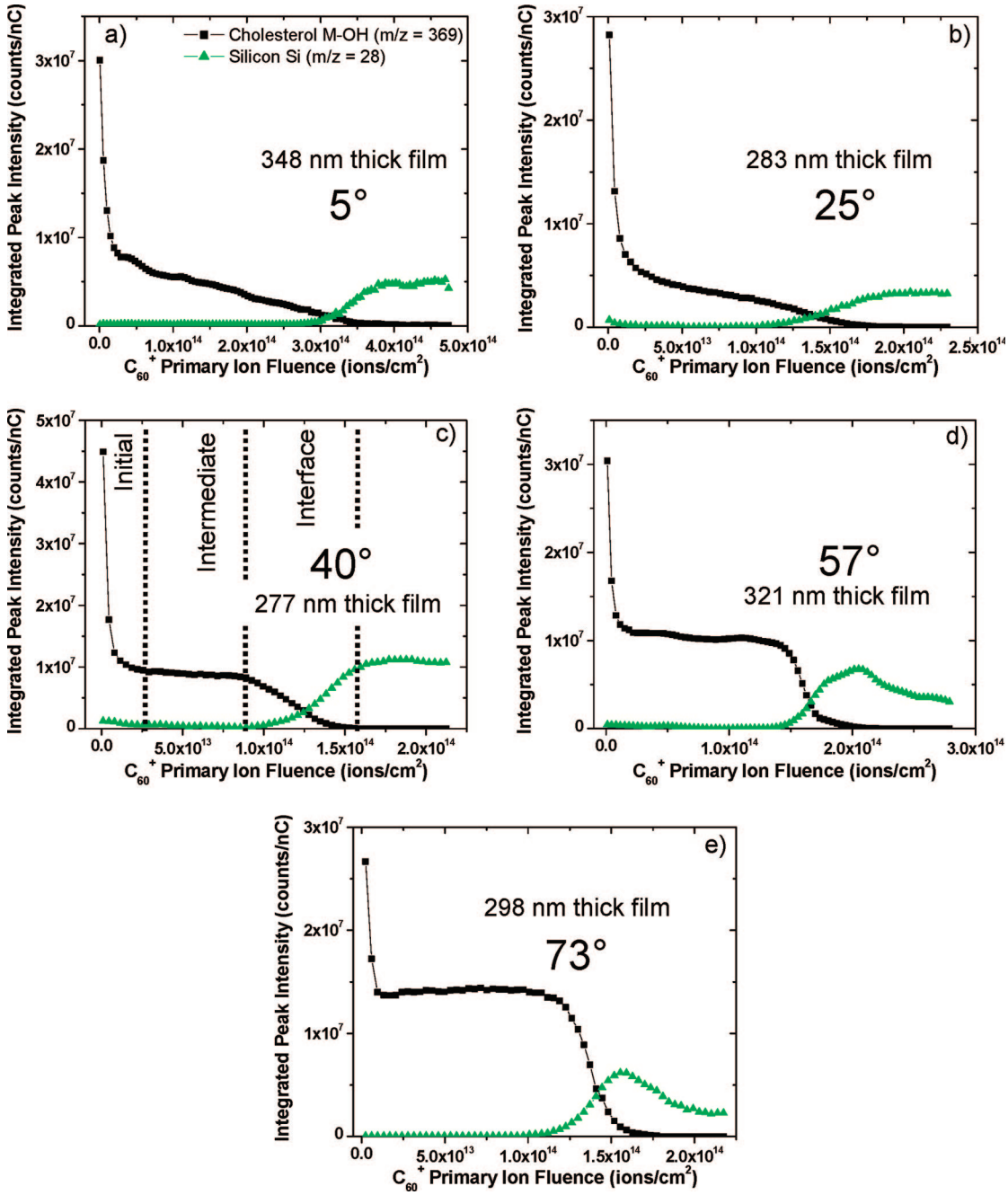

Figure 2. Depth profile plots of cholesterol quasi-molecular ion (m/z = 369, $[M-H_2O]^+$; black squares) and silicon (m/z = 28, Si^+, green triangles) ion intensities as a function of C_{60}^+ fluence. The depth profiles were acquired using 40-keV C_{60}^+ at 5° (a), 25° (b), 40° (c), 57° (d), and 73° (e) incidence. The three separate regions of the depth profile are labeled in (c). The silicon ion intensity is multiplied by a factor of 10 in each depth profile plot.

a single component system like the one studied here, $c_b = 1$. The quantity σ_D is the surface area damaged as a consequence of a single impact, often referred to as the damage cross section. More specifically, it is assumed that all molecules within a volume $d\sigma_D$ are destroyed per projectile impact. The first term in eq 1 describes the supply of undamaged molecules from the bulk into the altered layer due to the erosion process, while the second and third terms describe the loss of intact molecules from the altered layer due to sputtering and chemical damage, respectively. Ideally, eq 1 results in an exponential decay from an initial signal S_0 at zero fluence toward a steady state signal S_{ss} with a disappearance cross section $\sigma = Y^{tot}/nd + \sigma_D$, yielding

$$\frac{S_{ss}}{S_0} = \frac{Y^{tot}}{Y^{tot} + nd\sigma_D} \tag{2}$$

Since the degree of chemical damage decreases as S_{ss} approaches S_0, the relationship $Y^{tot} >> nd\sigma_D$ describes favorable conditions for molecular depth profiling. That is, chemical information is most effectively maintained during sample erosion when the total sputtering yield Y^{tot} (the number of cholesterol molecules removed per impact) is large relative to the number of

Table 1. Summary of Erosion Model Parameters Y^{tot}, $S_{ss}(0)/S_0$, σ_D, d, $Y^{tot}/nd\sigma_D$, Δz, $Y^{tot}(F)/Y^{tot}(0)$, a, and $Y^{tot}(0)$ as a Function of 40-keV C_{60}^+ Incident Angle Evaluated from the Depth Profile Data in Figure 2[a]

C_{60}^+ incident angle (±5°)	5	25	40	57	73
average sputter yield Y^{tot} (±32 molecule equiv)	305	420	503	470	425
$S_{ss}(0)/S_0$ (±0.06)	0.24	0.18	0.17	0.27	0.45
damage cross section σ_D (±5.5 nm^2)	12	23	33	32	22
altered layer thickness d (±4.1 nm)	63	56	42	22	13
cleanup efficiency ε (±0.09)	0.30	0.22	0.20	0.37	0.82
interface width δz (±6.1 nm)	40	36	32	22	25
$Y^{tot}(F)/Y^{tot}(0)$ (±0.04)	0.45	0.61	0.92	0.94	0.99
yield decay cross section a (±0.33 × 10^{-15} cm^2)	2.1	3.5	1.0	0.4	0.09
initial sputter yield $Y^{tot}(0)$ (±23 molecule equiv)	421	522	523	484	427

[a] The erosion model parameters are defined in the Discussion.

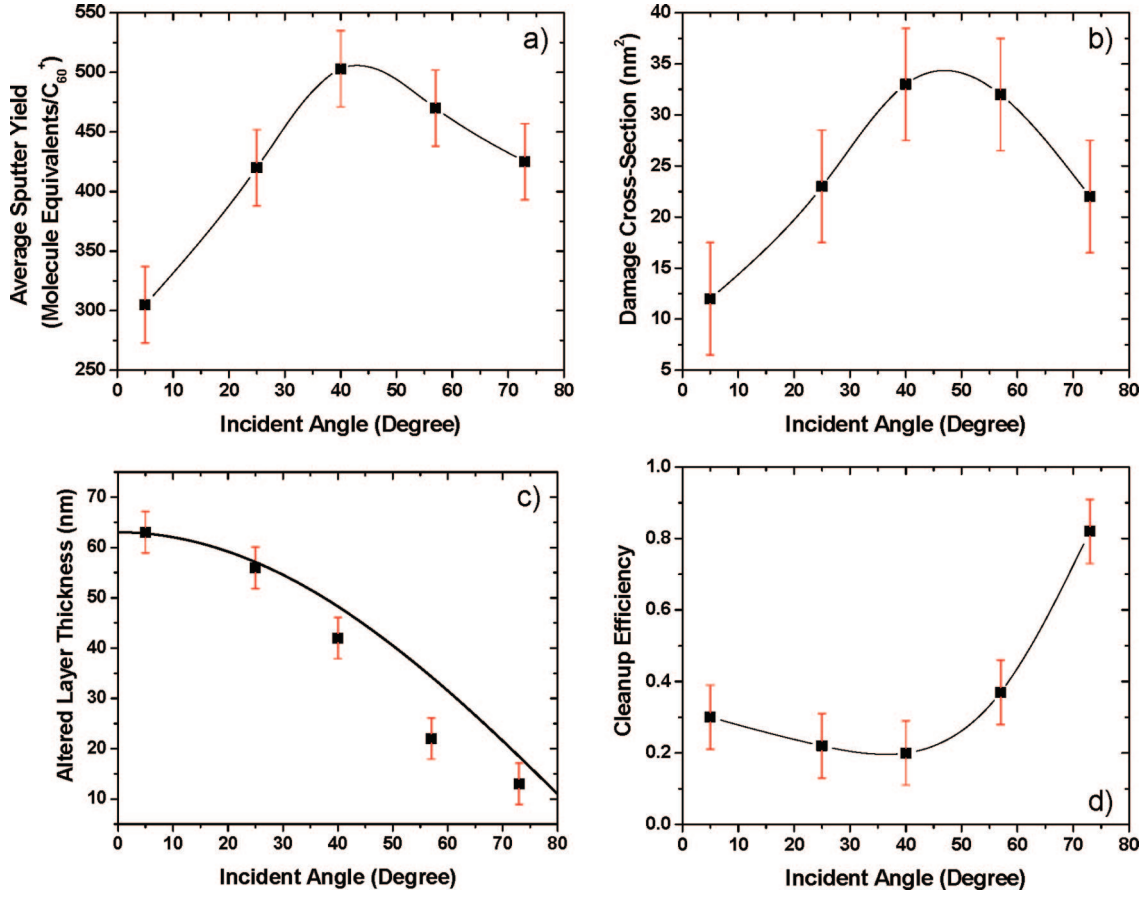

Figure 3. Summary of the erosion model parameters Y^{tot} (a), σ_D (b), d (c), and ε (d) as a function of 40-keV C_{60}^+ incident angle.

damaged molecules $nd\sigma_D$ within the altered layer. Accordingly, the depth profiles in Figure 2 are evaluated by calculating the depth profile parameters Y^{tot}, d, and σ_D and comparing Y^{tot} to $nd\sigma_D$ as a function of incident angle geometry.

Total Sputtering Yield. The dependence of total sputtering yield, Y^{tot}, on incident angle is calculated using the C_{60}^+ fluence required to remove an area of known thickness from the cholesterol film.[14,17,18,24] For example, the depth profile acquired at 40° incidence uses 1.53 × 10^{11} C_{60}^+ ions to remove 7.7 × 10^{13} cholesterol molecule equivalents, corresponding to a Y^{tot} of 503 cholesterol molecule equivalents per C_{60}^+ impact. The yields for the remaining geometries are summarized in Table 1 and in Figure 3. The values indicate that the yield increases from 305 at 5° to 503 at 40° before dropping off to 425 at 73°. The yield increase between 5° and 40° incidence is explained by the incident energy being deposited nearer the surface at more off-normal geometries, whereas the yield decrease between 40° and 73° incidence is explained by a fraction of the incident energy being reflected back into the vacuum at more glancing incident geometries. The yield trends agree well with MD simulations that examine the influence of incident angle on the 40-keV C_{60} bombardment of benzene.[27] The calculations predict that the yield correlates directly with the amount of energy deposited into the near-surface region of the solid. For example, bombardment at off-normal incidence deposits the energy most efficiently into the excitation zone, while bombardment at near-normal incidence deposits some of the energy too deeply into the solid. At glancing incidence, too much of the energy is reflected back into the vacuum.

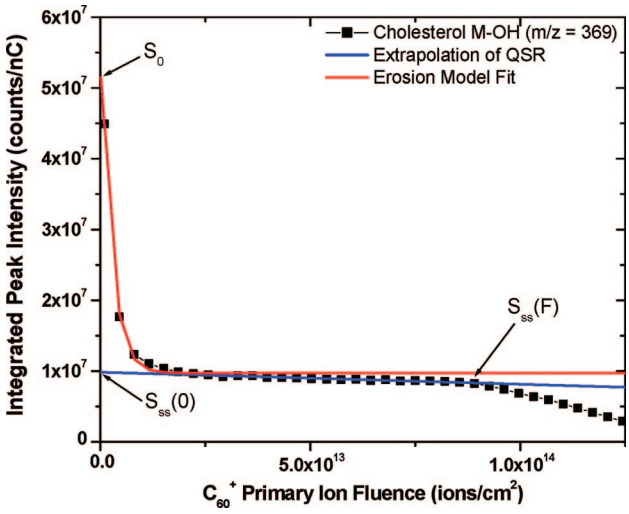

Figure 4. Extrapolation of QSR to zero fluence (blue line) and erosion model fit (red line) for the depth profile acquired using 40-keV C_{60}^+ at 40° incidence. The depth profile is a plot of cholesterol quasi-molecular ($m/z = 369$, $[M-H_2O]^+$; black squares) ion intensity as a function of C_{60}^+ fluence. The figure is representative of the fits used to calculate the erosion model parameters Y^{tot}, $S_{ss}(0)/S_0$, σ_D, d, ε, $Y^{tot}(F)/Y^{tot}(0)$, and a as a function of C_{60}^+ incident angle.

Damage Analysis. The damaged volume is determined from the product of the altered layer thickness d with the damage cross section σ_D.[14,18,28,30] To calculate these parameters, an exponential decay is fit to the cholesterol quasi-molecular ion signal ($m/z = 369$, $M - H_2O^+$) as a function of C_{60}^+ fluence in the low-fluence region as shown in Figure 4. The resulting disappearance cross section σ can then be used to determine σ_D via

$$\sigma_D = \sigma\left(1 - \frac{S_{SS}(0)}{S_0}\right) \tag{3}$$

However, a complication arises from the fact that not all depth profiles exhibit a true steady-state regime. At 5° and 25° impact angle, the main part of the depth profile where most of the film is removed is characterized by a relatively slow, almost linear decay of the steady-state signal S_{ss}. In these cases, the value $S_{ss}(0)$ to be inserted into eq 3 is determined by extrapolating the signal variation within the quasi-steady-state regime to zero fluence, also shown in Figure 4. Once σ_D, S_0, and $S_{ss}(0)$ are determined, the measured sputter yield Y^{tot} can be used to solve eq 2 for the unknown value of the altered layer thickness d. The resulting values for σ_D and d at each incident angle are summarized in Table 1 and in Figure 3. As a general trend, the damage cross section increases with increasing incident angle (except between 57° and 73°) while the altered layer depth decreases. The explanation for these trends is similar to the explanation for the yield trends. That is, as the incident angle increases from near-normal to glancing, the impact energy is deposited nearer the solid surface and along a greater surface area. The decrease in σ_D between 57° and 73° incidence is attributed to the reflection of energy back into the vacuum. The damage trends, particularly the trend for d, are consistent with MD simulations, which show that the impact crater formed by C_{60} at near-normal incidence is substantially deeper than the impact crater formed by C_{60} at glancing incidence—suggesting that the incident energy is indeed deposited nearer to the surface as the incident angle is increased.[27] If, as the conceptually simplest approximation, we assume the same "projected damage range" induced by the projectile impact irrespective of the impact angle θ, simple geometric considerations would suggest a $\cos(\theta)$ dependence of the altered layer depth. The corresponding curve is shown in Figure 3 and found to describe the observed trend rather well.

The yield and damage trends in Figure 3 and Table 1 suggest an interesting trichotomy in the relationship between the parameters Y^{tot}, σ_D, and d. Specifically, Y^{tot} is largest at 40° incidence while σ_D is smallest at 5° incidence and d is smallest at 73° incidence. To elucidate the seemingly conflicting values, the quantity $\varepsilon = Y^{tot}/nd\sigma_D$ was introduced as the efficiency for cleaning up the chemical damage produced in an impact event due to removal of the debris in the course of the same event.[30] The resulting cleanup efficiency calculated for each incident geometry is summarized in Table 1 and in Figure 3. The values indicate that the sputter yield relative to the number of damaged molecules per impact is least under 40° incidence and that this efficiency increases slightly toward normal incidence and substantially toward glancing incidence. Most importantly, the data clearly indicate that glancing incident geometries are most effective for maintaining chemical information during molecular depth profiling using 40-keV C_{60}^+. Moreover, the values indicate that the success of the experiment is not necessarily improved

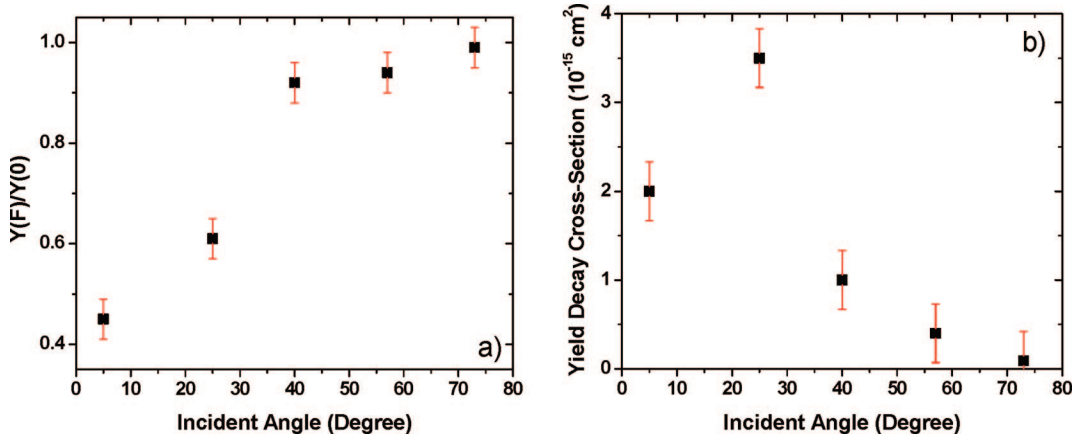

Figure 5. Summary of the QSR erosion model parameters (a) $Y^{tot}(F)/Y^{tot}(0)$ and a (b) as a function of 40-keV C_{60}^+ incident angle.

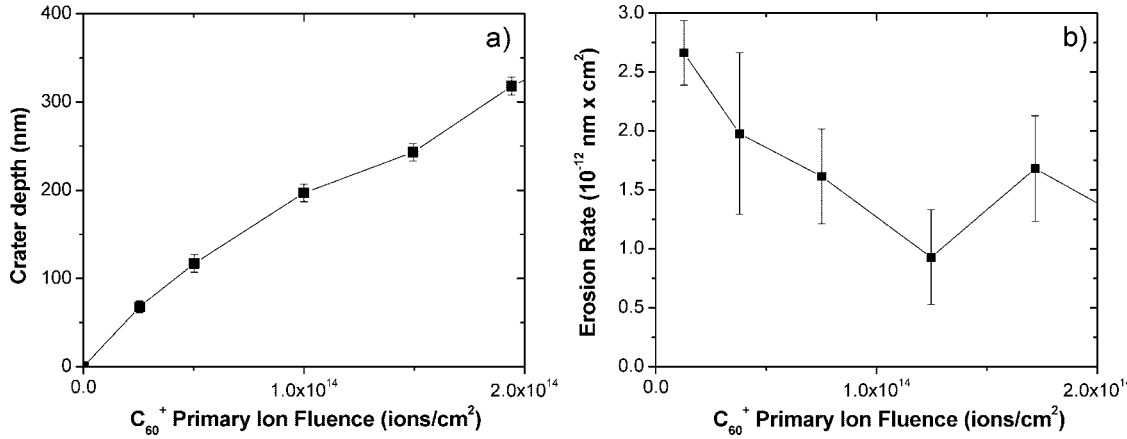

Figure 6. (a) Plot of eroded cholesterol film depth as a function of C_{60}^+ fluence. The plot was acquired using 40-keV C_{60}^+ at 5° incidence. The film depth was measured using AFM. (b) Plot of erosion rate as a function of C_{60}^+ fluence. The erosion rate is calculated from the slope of the plot in (a).

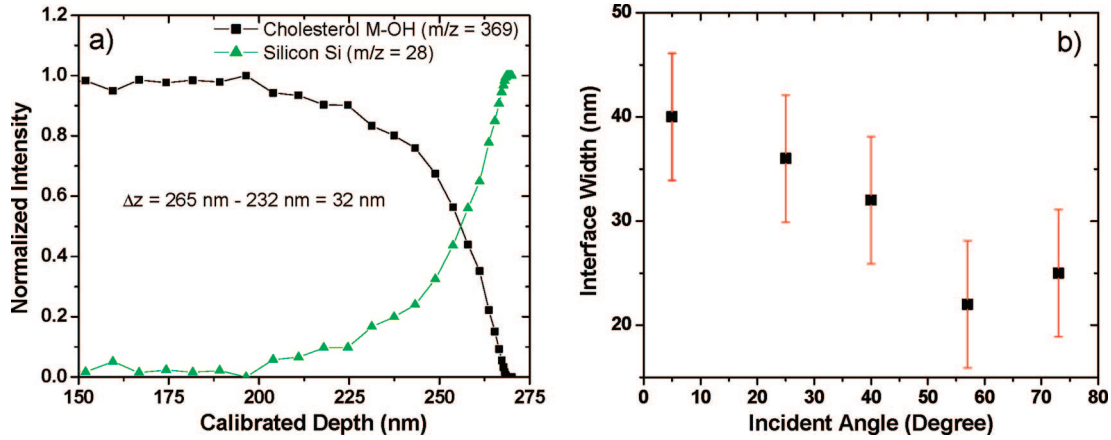

Figure 7. (a) Depth profile plot of cholesterol quasi-molecular ion ($m/z = 369$, $[M-H_2O]^+$; black squares) and silicon substrate ion ($m/z = 28$, Si^+; green triangles) normalized intensities as a function of calibrated film depth. The normalized intensities were calculated by taking the ratio of a specific ion intensity to the sum of the cholesterol and silicon ion intensities. The depth profile was acquired using 40-keV C_{60}^+ at 40° incidence and used to calculate the film/substrate 84%/16% interface width (Δz). The figure is representative of the depth calibration used to calculate Δz as a function of C_{60}^+ incident angle. (b) Summary of the erosion model parameter Δz as a function of C_{60}^+ incident angle.

by a larger sputter yield or smaller damage cross section but critically depends on the interplay between these quantities and the altered layer thickness. As for a general trend, molecular depth profiling seems to favor a smaller altered layer thickness.

Quasi-Steady-State Regime. As stated earlier in the discussion, the molecule response in the depth profiles in Figure 2 varies slightly according to the incident angle geometry. A particularly noticeable difference is the gradient of the signal loss in the intermediate quasi-steady-state removal region of each plot. In the depth profiles acquired using off-normal and glancing incident geometries, i.e., 40°, 57°, and 73°, a true steady-state region is discerned where the signal remains practically constant throughout the film removal. In contrast, depth profiles acquired using near-normal incident geometries, i.e., 5° and 25°, exhibit a substantial signal decay in this region. This observation is additional evidence that glancing incident angles are more effective for maintaining chemical information during erosion. The decay at near-normal incident geometries can be explained by a C_{60}^+ fluence-dependent decrease in the total sputtering yield. For that purpose, we extend the erosion model using the following assumptions in a fashion similar to that proposed recently by Shard et al.:[18]

- the measured molecular ion signal in the quasi-steady-state region (QSR) is given by

$$S \propto c_S Y^{\mathrm{tot}}$$

- the surface concentration c_s of intact molecules is described by

$$\frac{c_s}{c_b} = \frac{Y^{\mathrm{tot}}(f)}{Y^{\mathrm{tot}}(f)} + n d \sigma_D$$

Note that the second assumption represents an approximate solution of eq 1 if the fluence dependence of the total sputter yield is slow compared to the initial exponential signal decay. With these assumptions, the signal measured at a primary ion fluence f within the QSR is given by

$$\frac{S_{ss}(f)}{S_0} = \frac{Y^{\mathrm{tot}}(f)}{Y^{\mathrm{tot}}(f) + n d \sigma_D} \frac{Y^{\mathrm{tot}}(f)}{Y^{\mathrm{tot}}(0)} \tag{4}$$

Inserting eq 2 into eq 4, we obtain

$$\frac{S_{ss}(f)}{S_{ss}(0)} = \frac{x^2}{1 + S_{ss}(0)/S_0(x - 1)} \tag{5}$$

with $x = Y^{tot}(f)/Y^{tot}(0)$ describing the fluence dependent decay in total sputter yield and S_0 and $S_{ss}(0)$ being defined above (see Damage Analysis). Note that eq 5 contains only measured data, which can be extracted directly from the depth profile. As a consequence, the sputter yield decay throughout the QSR can be determined by solving eq 5 for x. The resulting decrease in sputter yield between the zero fluence value and that at the fluence F immediately before reaching the interface is depicted in Table 1 and in Figure 5. It is seen that a sizable effect occurs only at near-normal incidence geometries, where the data evaluation performed here predicts the sputter yield to drop to about half of its initial value during the film removal. Assuming, as a first approximation, a linear decrease according to

$$Y^{tot}(f) = Y^{tot}(0)(1 - af) \tag{6}$$

a decay cross section, a, is obtained for each depth profile. The values are summarized in Table 1 and in Figure 5. In this approximation, the average sputter yield throughout the removal of the entire film is given by

$$Y^{tot} = \frac{Y^{tot}(0) - Y^{tot}(F)}{2} = Y^{tot}(0)\frac{1 + (1 - aF)}{2} \tag{7}$$

Since this quantity is known from the fluence needed to remove the film, the initial yield $Y^{tot}(0)$ at zero fluence can be determined by solving eq 7 using the known values of F and a. The resulting values are also depicted in Table 1. Note that $Y^{tot}(0)$ needs to be inserted into eq 2 in order to arrive at accurate values of the altered layer thickness. The values for d listed in Table 1 have been corrected accordingly. Together, the values for $Y^{tot}(F)/Y^{tot}(0)$ and a support the earlier qualitative observation that the total sputtering yield decrease in the QSR is largest at near-normal incident angle geometries and smallest at off-normal and glancing incident angle geometries.

It should be noted that a more general formulation of the erosion dynamics model should incorporate a fluence-dependent exponential decrease of the total sputter yield inserted into eq 1. However, the resulting differential equation cannot be solved in closed form for arbitrary parameters. If a is small compared to both σ and the inverse film removal fluence $1/F$, the yield decay can be approximated by eq 6 over the fluence range of interest and the model predicts the same approximate solution derived above.[39]

Sputter Yield Measurements as a Function of C_{60}^+ fluence. To examine the idea of a sputter yield reduction across the QSR, a cholesterol film was bombarded to various depths using 40-keV C_{60}^+ at 5° incidence. The eroded depth was measured using AFM and is reported as a function of C_{60}^+ fluence in Figure 6. The sputter rate during each fluence increment was then calculated by determining the slope of the depth versus fluence response over that increment. The erosion rate as a function of C_{60}^+ fluence is reported in Figure 6. As expected, the value, which is proportional to the total sputtering yield, decreases with increasing C_{60}^+ fluence, thus supporting our interpretation of the QSR signal variation. The reason for the observed yield behavior is currently unclear. Possible explanations of the decay in the QSR involve a fluence-dependent "chemical poisoning effect" that is attributed to chemical damage accumulation and/or C deposition.

The last data point depicted in Figure 6 corresponds to the interface region near the silicon substrate. We speculate that the increase in yield at this point may arise from reflection of energy at the substrate surface.

Interface Width. To verify the concept developed above, the broadening of the interface region between the cholesterol film and the silicon substrate during C_{60}^+ erosion is examined. In the absence of topological effects, the interface width Δz should be a measure of the damaged depth within the solid.[13,29,30,38] To calculate Δz, the fluence scale must be converted to a depth scale by correcting for the varying erosion rates through the film/substrate interface.[29,30] As a first approximation, the overall erosion rate $\dot{z}$ is linearly interpolated between the values $\dot{z}_{Chol}$ and $\dot{z}_{Si}$ of the pure cholesterol film and the silicon substrate, respectively. This is done using both the variation of the film signal S_{Chol} (at m/z 369) and the substrate signal S_{Si} (at m/z 28) according to

$$\dot{z} \cong c_{Chol}\dot{z}_{Chol} + c_{Si}\dot{z}_{Si} \tag{8}$$

with weighing factors

$$c_{Chol} = \frac{S_{Chol}/S_{Chol}^{max}}{S_{Chol}/S_{Chol}^{max} + S_{Si}/S_{Si}^{max}} \quad \text{and} \quad c_{Si} = \frac{S_{Si}/S_{Si}^{max}}{S_{Chol}/S_{Chol}^{max} + S_{Si}/S_{Si}^{max}}$$

where S is the integrated peak intensity of the indicated species and S^{max} denotes the respective maximum signal detected throughout the entire depth profile. In the case of S_{Chol}, we use the quasi-steady-state signal extrapolated to zero fluence for S^{max} in order to account for the initial signal drop caused by chemical damage. The silicon erosion rate was estimated using measured sputter yield data determined from eroding craters into a clean silicon surface.[40] The actual value of $\dot{z}_{Si}$, however, is not important since in all cases $\dot{z}_{SI} << \dot{z}_{Chol}$, thus rendering silicon erosion practically negligible. Then, the cholesterol erosion rate is determined by integrating eq 8 over the entire depth profile and equating the result to the total eroded depth measured from the AFM crater profile. A complication arises at near-normal incidence, where $\dot{z}_{Chol}$ is not constant throughout the film removal. In these cases, we assume the erosion rate to decay linearly with the same cross section as determined for the total sputter yield (see Table 1). Using the corrected sputter rates, the fluence data can be converted to a depth scale as shown, for instance, for the depth profile acquired under 40° incidence in Figure 7. The parameter Δz is then estimated as the depth interval between 84 and 16% of the maximum silicon intensity. The values for Δz as a function of incident angle are summarized in Table 1 and in Figure **7**. The values indicate that Δz decreases from 40 nm at 5° incidence to 25 nm at 73° incidence. Hence, glancing incident geometries do in fact confine the damage nearest the solid surface during sample erosion. Moreover, the best depth resolution is achieved when glancing incident geometries are used for molecular depth

(39) Wucher, A. Surface and Interface Analysis, submitted.

(40) Kozole, J.; Winograd, N. *Appl. Surf. Sci.* In press.

profiling. However, it is interesting to note that the depth resolution of the experiment is limited to ~20 nm, a value much greater than the 5-nm intrinsic roughness of the film. The reasons behind the film/substrate interface broadening are currently under investigation.

CONCLUSIONS

Molecular depth profiles at incident angles ranging from 5° to 73° using 40-keV C_{60}^+ show that as the incident angle increases the cleanup efficiency increases, the yield decay cross section in the QSR decreases, and the interface width decreases. Therefore, glancing incident geometries, such as 73°, deposit the incident energy in a location within the solid most effective for maintaining chemical information during sample erosion using 40-keV C_{60}^+. The finding is attributed to the incident energy being deposited nearer the solid surface at glancing incident angles resulting in a decrease in altered layer thickness that apparently more than offsets any concomitant decrease in total sputtering yield or increase in damage cross section. Therefore, as a general rule, the key to a successful molecular depth profile is to deposit the most amount of energy as possible in the near-surface region of the solid using a single projectile. Under this condition, it is expected that the bulk of the damaged molecules will eject during the impact event and any residual molecule damage will remain close to the sample surface allowing it to be easily removed by subsequent bombardment. Thus, projectiles with a large number of constituent atoms, such as C_{60}^+, at large kinetic energies, such as 40 keV, and glancing incident angles, such as 73°, are most appropriate for molecular depth profiling.

ACKNOWLEDGMENT

The authors acknowledge the National Institute of Health under grant EB002016-13, the National Science Foundation under grant CHE-0555314, and Department of Energy under grant DE-FG02-06ER15803 for partial financial support of this research. The authors also acknowledge David Willingham for sample preparation and Barbara J. Garrison and Kathleen E. Ryan for helpful discussion.

Received for review February 12, 2008. Accepted May 5, 2008.

AC8002962